EUV and non-EUV inspection of reticle defect repair sites

Kenneth A. Goldberg[1], Anton Barty[2], Phillip Seidel[3], Klaus Edinger[4], Rainer Fettig[4], Patrick Kearney[5], Hakseung Han[5], Obert R. Wood II[6]

[1]Center for X-Ray Optics, Lawrence Berkeley National Laboratory, Berkeley, CA 94720, USA
[2]Lawrence Livermore National Laboratory, Livermore, PO Box 808, CA 94550, USA
[3]SEMATECH, 2706 Montopolis Drive, Austin TX 78741, USA
[4]Carl Zeiss SMS, Industriestr. 1, 64380 Rossdorf, Germany
[5]SEMATECH, 255 Fuller Road, Suite 309, Albany, NY 12203, USA
[6]Advanced Micro Devices, 255 Fuller Road, M/S 253, Albany, NY 12203 USA.

ABSTRACT

We report the actinic (EUV wavelength) and non-actinic inspection of a multilayer-coated mask blank containing an array of open-field defect repair sites created in different ways. The comparison of actinic brightfield and darkfield measurements shows the importance of having both local reflectivity and scattering measurements. Although effective mask blank repair capabilities have not been adequately demonstrated, the data acquired in this experiment have been very instructive. Correlation with non-actinic inspection methods shows the difficulty of establishing a successful predictive model of the EUV response without EUV cross-comparison. The defect repair sites were also evaluated with SEM, AFM, and 488-nm-wavelength confocal microscopy. The data raise important questions about mask quality specifications and the requirements of future commercial actinic inspection tools.

Keywords: extreme ultraviolet lithography, EUV, mask inspection, defect repair, actinic inspection.

1. INTRODUCTION

The production of defect-free mask blanks for extreme ultraviolet (EUV) lithography requires the development of mask inspection tools of unprecedented sensitivity and defect repair techniques that are suitable for the highly sensitive reflective surface of EUV reticles. We have developed a unique actinic mask inspection tool[1,2] that operates at EUV wavelengths and is now used in the evaluation of patterned and open-field defect repair strategies without printing[3,4]. The tool is also being used to deepen our understanding of the sensitivity of non-actinic inspection methods, and to resolve research questions about the development of, or need for, commercial actinic tools[3,5].

It is well known that the resonant reflectivity of EUV multilayer coatings is highly sensitive to any disturbance of the coating surface or layer structure: including substrate bumps and pits which cause phase-defects, and absorbing particles or surface material which causes local reflectivity loss. Multilayer defect repair efforts seek to restore the local optical properties of the multilayer and minimize the impact of coating imperfections on printed patterns. The development of successful defect repair techniques requires detailed feedback that, realistically, can only come from at-wavelength evaluation. EUV printing can be an effective evaluation technique for defects in the absorber pattern, but it is unlikely to provide accurate, quantitative feedback for open-field defect repairs. Non-EUV inspection tools may be able to verify the restoration of the top surface quality, but they are largely insensitive to the multilayer properties that determine the EUV reflectivity. Furthermore, the penetration depths of UV light into EUV multilayers can be very shallow, as described in Section 2, meaning that other light wavelengths behave like surface probes for multilayer coatings.

To evaluate different multilayer defect repair methods and recipes, we have recently inspected defect repair sites on an EUV mask blank with the SEMATECH actinic mask inspection tool at Lawrence Berkeley National Laboratory. We used both actinic brightfield (BF) and darkfield (DF) detection with sub-micron spatial resolution and sensitivity to reflectivity variations as small as 0.2%. The BF signal measures local reflectivity changes, while the DF signal records the scattered-light amplitude. Interestingly, some repair sites that exhibit substantial BF reflectivity losses have low DF scattering strengths. We believe that local light absorption plays an important and possibly under-appreciated role in these

Emerging Lithographic Technologies XI, edited by Michael J. Lercel,
Proc. of SPIE Vol. 6517, 65170C, (2007) · 0277-786X/07/$18
doi: 10.1117/12.712202

cases. Furthermore, we did not observe a strong predictive correlation between DF scattering and BF reflectivity loss. This point has important implications for the design of next-generation EUV mask inspection tools.

We present the cross-calibration of the EUV measurements with atomic force microscopy (AFM) data, and we correlate the available data with both scanning electron microscopy (SEM) measurements and defect review images collected on a 488-nm commercial mask blank inspection tool.

2. LIGHT PENETRATION INTO EUV MULTILAYERS

Multilayer coatings are by nature resonant structures that create strong reflectivity by forming a deeply penetrating standing wave at the design wavelength. For significantly longer wavelengths, the field resonance is not supported and the multilayer behaves more like a single material of an intermediate index value**.** A study of the light intensity penetration into an EUV multilayer structure reveals the extent to which UV inspection serves as a surface probe, limited only to the top few layers of the multilayer.

Figure 1 shows the calculated light penetration intensity for three wavelengths into a 40-bilayer Mo/Si EUV multilayer mirror optimized for normal incidence reflection at 13.4-nm wavelength. The wavelengths of interest are the design wavelength, 13.4 nm, and two UV wavelengths used in commercial mask-blank inspection tools, 266 nm and 488 nm. For simplicity, the simulation uses sharp layer interfaces, a Si top layer, and a thick Si substrate for the bottom layer. TEMPEST 6.0[6], which uses the finite-different time-domain method to solve Maxwell's equations for the vector electromagnetic field, was used to calculate the field intensities in a 1-D geometry using a 0.2-nm node spacing.

Penetrating into the material, the EUV wavelength shows a clear standing wave matching the periodicity of the layer structure, and exponential decay. The UV wavelengths show only rapid exponential attenuation and only penetrate tens of nm. The field strengths are normalized to a unit input intensity. A difference in reflectivity accounts for the abrupt drop in intensity at the surface for the two UV wavelengths. The field parameters are described in Table 1.

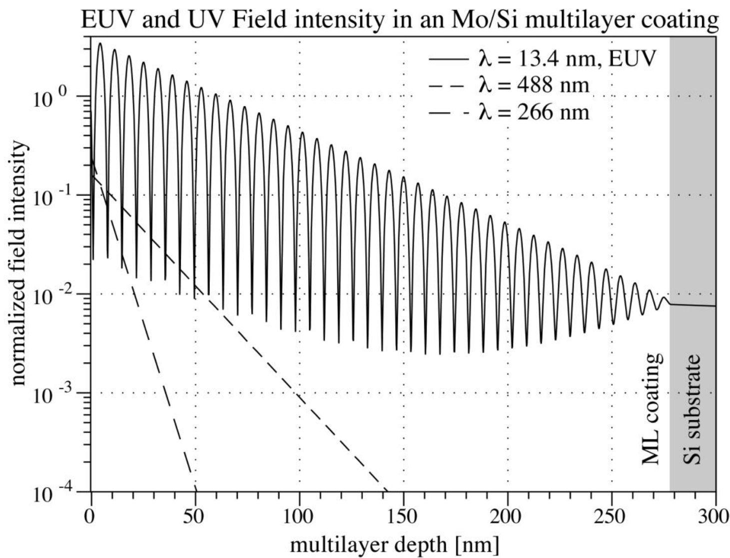

Fig. 1. Calculated light penetration intensity into an ideal EUV multilayer coating for three different wavelengths at normal incidence. The coating period $d = 6.940$, and $\Gamma = 0.394$.

Table 1. Light-intensity penetration parameters for three wavelengths of interest to EUV mask inspection. The "1% depth" refers to the depth at which the field intensity reaches approximately 1% of the incident value; the numbers of bi-layer pairs corresponding to those depths are also given.

λ	*R*	1% depth	bi-layers
13.4 nm	72.7%	215 nm	31
488 nm	58.4%	53.6 nm	8
266 nm	41.9%	20.6 nm	3

The rapid attenuation of the non-actinic wavelengths, compared to the deep penetration of the EUV field, provides one of the strongest motivations for the continued development of EUV inspection techniques. Until inspection differences are well understood, or multilayer smoothing technologies have evolved where the UV inspection wavelengths can predict the EUV response, ongoing cross-correlation studies will be necessary.

3. DEFECT REPAIR MASK

A number of repair strategies have been proposed to address pattern defects[7,8] and, separately, open field *phase* defects[9]. The open field repair strategies have included attempts to induce local compaction of the coating and substrate and a different approach applied here to "scoop out" a problematic section of the multilayer.

A multilayer-coated EUV mask blank (serial number 615PUQ19) was prepared containing an array of fourteen defects and repair sites. The mask blank was coated by the SEMATECH North Mask Blank Development Center (MBDC). The repair involved an e-beam-activated chemically induced etching process that can be localized very controllably at the size of the defect. The process was developed by Carl Zeiss SMS and performed on a mask repair tool prototype. The goal was to create repairs with sidewall slopes below 4°, which has been calculated as the largest acceptable angle that does not create phase shift errors[10]. Repairs were performed in an open loop procedure (not using feedback) without tight control of surface roughness. The measurements contained here provide very interesting results to improve the process.

Circular marks of similar in size and configuration were etched into the mask and treated in three different ways to distinguish effects of the etching into the multilayer from the effects of a protection layer. The etch and repair site diameters varied from 2 to 6 µm. The sites were assigned letters A through N, and are grouped as follows. The available preparation details are in Table 2.

Group I, defects A–E: Sites were etched as ditches (pits) with shallow sidewall angles in the range of 2° to 4°.

Group II, defects F–J: SiO_2 was deposited in different thicknesses, of approximately 1.5–12 nm.

Group III, defects K–N: Defects were etched into the top layer, to different depths, and the area was covered with a SiO_2 *protection layer* approximately 5-nm thick, with a larger diameter.

Table 2. Brief descriptions of the repair site preparation methods for the fourteen sites on the mask. Sidewall angles and layer thicknesses are estimated values.

Group I sites	ditches: maximum diameter, sidewall	**Group II** sites	SiO_2 deposition approx. thickness	**Group III** sites	etch region diameter, protection-layer diameter
A	2 µm, 3°	F	12 nm	K	4.2 µm, 5 µm
B	4 µm, 3°	G	1.5 nm	L	5.0 µm, 6 µm
C	4 µm, 3°	H	8 nm	M	4.2 µm, 5 µm
D	4 µm, 3°	I	4 nm	N	4.2 µm, 5 µm
E	4 µm, 2°	J	6 nm		

4. MEASUREMENTS AND CORRELATION

The defect repair sites were measured with several available techniques including EUV BF (reflectivity) and DF (scattering) scanning, AFM, SEM, and defect review mode of the Lasertec M1350, which operates at 488-nm wavelength. Seven SEM images are available from sites in each group. AFM measurements were made to characterize the 3-D shape of the repair sites in Groups II and III. The other tools are described below, and the measurement data are compiled in Figs. 2 through 4.

4.1 Actinic inspection

The SEMATECH actinic inspection tool at Lawrence Berkeley National Laboratory[1,2,3] is a dual-mode microscope designed for *at-wavelength* inspection of EUV reticles. The tool has been described previously; however several recent upgrades have improved its performance. It operates on a bending magnet beamline at the Advanced Light Source with a monochromator that provides an energy bandwidth of $\Delta E/E \sim 1/1000$. Operating in *zone-plane imaging mode*, the tool emulates the optical properties of a 0.25-NA stepper and functions as a high-resolution microscope, recording the aerial image reflected from the mask. In *scanning mode*, used to obtain data for this study, a focused beam with 6° angle of incidence illuminates a tiny section of the upward-facing reticle surface, with a diameter as small as 1 µm. A pair of EUV photodiodes separately captures the BF specular reflection and a limited solid angle of the DF scattered light as the mask is translated below the stationary beam. In this manner, scanning mode operation is analogous to a high spatial resolution EUV reflectometer, probing the surface optical properties micron by micron. The DF detector directly captures an off-axis angular range from approximately 0.6°–35° in one direction, and ±4.3° in the perpendicular direction.

Recent upgrades replaced the original detector geometry that was significantly less photon-efficient due to the presence of a 48° multilayer-coated turning mirror. The mirror's limited angular bandpass reduced the collection solid angle significantly. Scattering also caused light from the BF specular beam to overlap the sensitive micro-channelplate used as the DF detector, thereby reducing the sensitivity to small signal changes. The new photodiode detectors are positioned above the mirror surface, efficiently collecting the reflected light without intervening mirror elements.

We have observed that the signal-to-noise properties of DF data collection benefit by using a somewhat larger scanning beam; a 5-µm diameter was used in these measurements. The BF signal gains more spatial discrimination and sensitivity when a smaller beam is used; for those measurements, we performed separate scans with a 1-µm diameter beam.

Figure 2 contains data from the actinic measurement of all fourteen sites. The key statistics are the peak reflectivity loss, labeled "BF ΔR" and the DF signal strength, labeled "DF SNR." The BF relative reflectivity data are normalized to the clear mirror areas adjacent to the defect sites. We report both the local observed (relative) reflectivity loss (with 1-µm resolution), and the complementary relative reflectivity, labeled simply "R."

The DF signal is handled differently. At each site, the measured DF signal is offset to achieve a zero average value in the area outside the repair site. The signal from an 8.1-µm square area containing the repair site is then integrated to produce a response-strength value. We report this value normalized to the standard deviation of the measured background (i.e. the RMS for 8.1-µm square regions). The value we report is thus the signal-to-noise ratio (SNR) of the measured defect site. This data is labeled "DF SNR" in Fig. 2. Some defect sites scattered light strongly, making a large DF signal. For other sites, the scattered light signal was *lower* than the surrounding area. Those sites are reported as negative values.

4.2 Lasertec M1350 inspection

The Lasertec M1350 uses an argon-ion laser at a 488-nm illumination wavelength. The scanning confocal system uses a *multiple image acquisition for Giga-bit Inspection with confocal system* (MAGICS) configuration to achieve both high throughput and sensitivity. On transparent mask substrates, the M1350 can scan the entire 200 cm^2 quality area in 20 minutes; it has previously demonstrated polystyrene latex (PSL) equivalent-size sensitivity below 60 nm[5,11,12].

The authors note that this mask experienced significant spontaneous etching of the top layer in areas not processed. This overetching is visible in SEM images as small dots and as small craters in the etched areas. For this reason, and separate concerns about possible particulate contamination, the M1350 inspection was not performed in scanning mode. Instead thirteen of the sites were inspected using a *defect review* mode that captures an image of the site with differential contrast. The sites were readily apparent in this mode, and although scanning was not performed, the primary tool operator believed that all of the sites would have been detected easily.

4.3 Available data

Data collected using the different measurement techniques is shown in Figs. 2, 3, and 4. The repair sites are clearly visible in the M1350 data despite the varying degrees of contrast. Sites G and I, which have the weakest apparent contrast, also have the least top surface height deviation, among the sites that were measured in the AFM, and the smallest change in EUV reflectivity. Site K, on the other hand, appears to be a deep circular ditch, 71 nm lower than the surrounding area. This site shows very high M1350 contrast and caused the strongest EUV signal changes.

4.3.1 Actinic BF vs. DF signals. Figure 3 shows the correlation between the actinic BF and DF signals for the fourteen sites. The data are clustered into three distinct groups, following their preparation type, except for the Group III sites, which show two different behaviors. The Group I sites all show both significant local reflectivity loss and strong scattering strength. It is possible that changes in the surface angle resulting from the creation of shallow ditches steer the reflected light by small angles, or the rough surface created by the open-loop etching may scatter the beam. In contrast, the negative DF scattering values for the Group II sites seem to imply that the local SiO_2 deposition is responsible for light absorption with reduced scattering. The four Group III sites show two very different EUV responses. With their suppressed scattering, it is possible that in cases L and M, the etching did not penetrate the top layer, causing them to behave more like Group II sites. However, sites K and N, where the etch may have penetrated the top layer, show the strongest reflectivity losses and the highest scattering strengths. These similarly prepared sites are very likely deep pits.

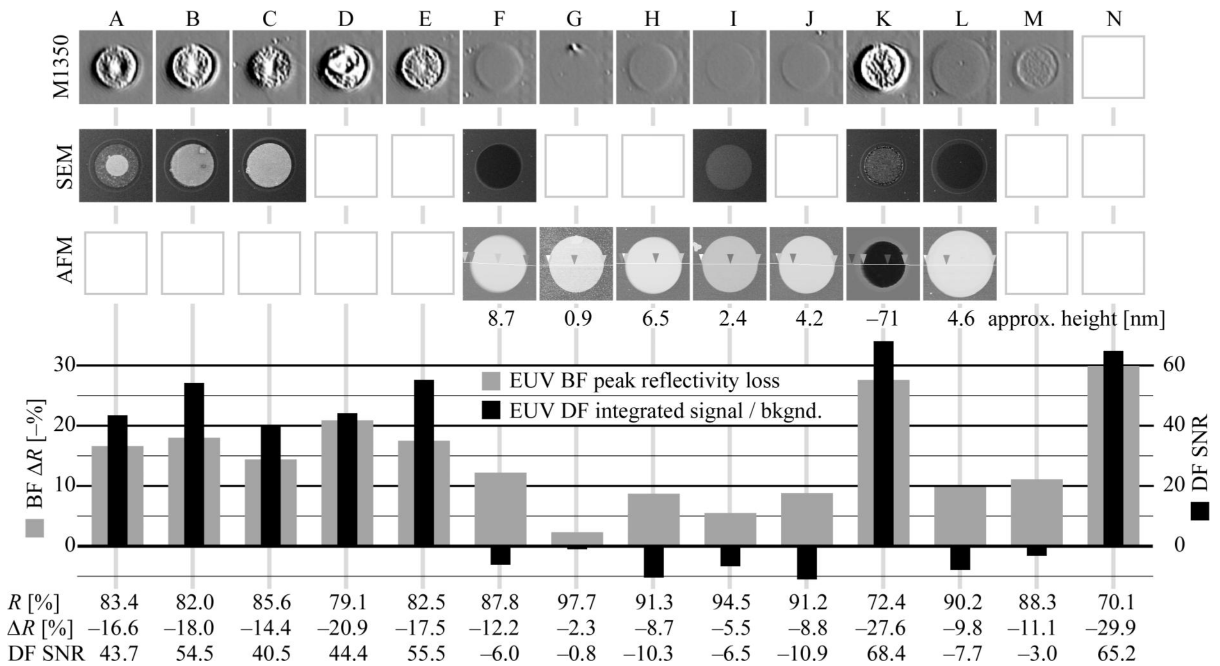

Fig. 2. Summary of the available measurement data for the fourteen sites of interest. Group I is A–E, Group II is F–J, and Group III is K–N. The data include SEM, AFM, defect review confocal microscopy at 488-nm wavelength (labeled M1350), and actinic BF and DF signals. Unavailable data are indicated with an open square. The AFM data shows a range of top-surface heights for the sites that were studied. The EUV response is highly varied, as discussed in Figs. 3 and 4.

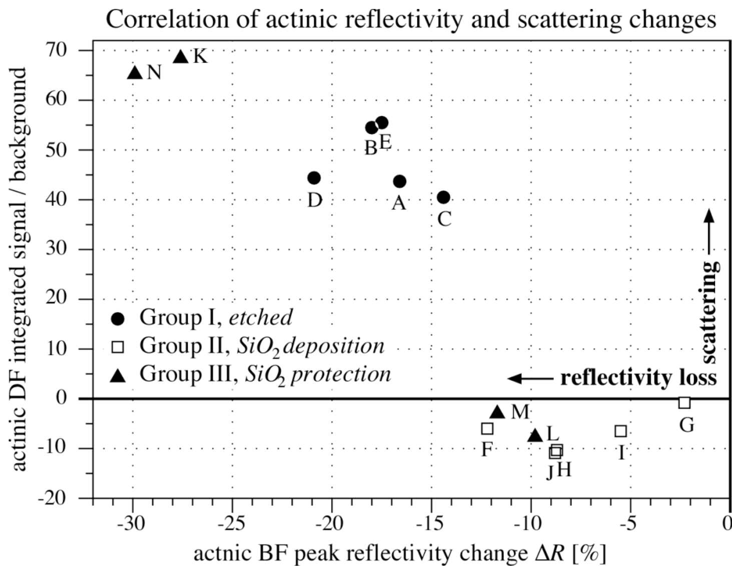

Fig. 3. Actinic BF and DF signal for each of the fourteen sites. No single trend emerges. The shallow ditches of Group I show strong scattering with reflectivity losses. Group II sites also showed reflectivity losses, yet had suppressed scattering levels, suggesting absorption.

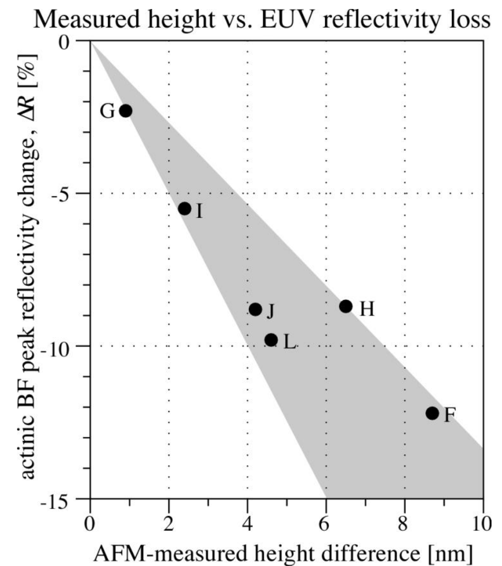

Fig. 4. Observed changes in EUV reflectivity vs. measured AFM height change at surface. There is a broad trend of lowered EUV reflectivity with the additional SiO_2 thickness.

The range of observed EUV behaviors described here has serious implications for actinic inspection tools. The imperfect correlation between BF and DF signal changes shows us that actinic inspection tools designed to measure only the DF scattering strength risk missing sites associated with significant reflectivity losses. However, these measured reflectivity changes are much greater than 1%, so the relevance of this poor correlation to masks in a production environment is questionable.

4.3.2 Actinic BF vs. SiO_2 deposition thickness. Figure 4 shows the correlation between the AFM-measured surface height and the local loss of EUV reflectivity. Since the surface height follows the thickness of the deposited SiO_2, it is not surprising that the trend is for decreased reflectivity with increased SiO_2 thickness. The upper and lower borders of the gray shaded region correspond to the lines defined by ΔR [%] = – 1.33 h [nm] and ΔR [%] = –2.5 h [nm], respectively. Roughly, we lost 1% reflectivity for each 2 nm of SiO_2. Note that the data point for site K (–71 nm, -27.6%) also fits within the trend area, but was excluded from the plot.

5. DISCUSSION

The EUV optical properties of multilayer surfaces are highly sensitive to the local surface conditions and have a unique response to any illuminating wavelength. EUV light penetrates deeply into the multilayer coating structure, probing subtle disruptions in the resonance-producing properties, while UV light wavelengths used in commercial mask inspection tools reach only into the top several bi-layers.

The defect repair treatment methods studied here did give very valuable insight for future improvement of the repair process. The value of performing such actinic measurements in concert with repair efforts is evident in the unexpected results. The data presented here show the importance of cross-correlation experiments, yet they raise a number of questions about future directions and inspection requirements. So little data of this kind currently exists; additional research is clearly necessary.

5.1 The need for micron-scale BF and DF actinic inspection

The micron-scale repair sites fall into an interesting, intermediate measurement length scale. With sizes that are three or four orders of magnitude smaller than the area of the typical beam footprint in an EUV reflectometer, the EUV properties of such sites can be studied effectively only by moderately high spatial resolution actinic tools (micron-scale), such as the SEMATECH actinic inspection tool in Berkeley, or other tools being developed elsewhere[13,14,15].

The data suggest significant risks are associated with limiting an actinic inspection tool to just BF or DF mode alone. For example, a system with only DF detection may have high sensitivity to small bumps and pits, but may miss significant absorptive defects completely, especially when they occur with micron length scales. On the other hand, a system with only BF detection could not rely on the enhanced discrimination provided by scattering to improve the detection of small but relevant defects.

Optimizing actinic detection geometries for both DF and BF signals is a significant challenge. For example, in the Berkeley tool, BF measurement with high spatial resolution requires a tightly focused beam. We measure variations in the specular reflected beam, and when a defect's area is significantly smaller than the beam footprint, we can expect only a small signal variation. On the other hand, the DF scattered light signal is generally very weak and requires as much available light as possible. To improve DF detection, we have found that it helps to illuminate the mask with a slightly larger beam area (we use up to a 5-µm diameter), giving up some spatial resolution. Because of this BF and DF difference, it can be challenging to simultaneously optimize conditions for the detection of both signals. This difficulty could also become important for actinic inspection tools built on the principle of a large area imaging microscope of modest spatial resolution. With an annular pupil, as in the MIRAI tool[13], DF collection efficiency is very high owing to the large collection solid angle and blocking of the specular beam. However, if the BF signal were to be recorded in a similar manner, flare in the imaging lens, combined with the low spatial resolution, could overwhelm the signal variations caused by small opaque defects.

5.2 Consideration of the SEMI P38 standard

Finally, it is worthwhile to consider the mask blank and multilayer coating quality specifications described in the current SEMI P38 document[16]. The standard calls for EUV measurements to assess reflectivity within a "rectangular dimension of < 1 mm." At this coarse inspection length scale, it seems likely that all or most of these defect repair sites studied here would be missed; such a mask would pass qualification despite their presence. Regarding coating uniformity, SEMI P38 (Table 6) calls for a "maximum range of peak reflectivity (absolute)" to be at or below 1.2%, and down to 0.5% for *Class A* masks. However, little guidance is given as to the allowed spatial scale of the variation, including the possibility of abrupt changes that would likely affect the aerial image. Of the defect repair sites studied in this report, *all of them* far exceed even the Class D uniformity standard.

With the demonstrated possibility of subtle damage to the coating reflectivity caused by mask inspection[4], and the possibility of small-scale damage caused by future defect repair tools, the spatial scale over which reflectivity changes occur seems to be a critical unaddressed issue deserving continued research. In the SEMATECH Berkeley tool, we have observed inspection damage, in the form of percent changes in EUV reflectivity, induced by SEM, UV, and focused-ion beam inspections. In several cases, these effects have been visible only with actinic inspection and/or EUV lithographic printing. Damaged regions can appear as narrow lines or rectangular regions with lowered reflectivity.

ACKNOWLEDGMENTS

The authors gratefully acknowledge Yanwei Liu for his central role in the development of the actinic inspection tool, and Senajith Rekawa and C. Drew Kemp for expert engineering and technical support. Eric Gullikson and Erik Anderson, of LBNL, and John Taylor of LLNL provided many helpful insights. This work was performed under the auspices of the U.S. Department of Energy by University of California Lawrence Berkeley National Laboratory, and Lawrence Livermore National Laboratory, and was funded by SEMATECH under Project LITH-343.

REFERENCES

1. A. Barty, Y. Liu, E. Gullikson, J. S. Taylor, and O. Wood, "Actinic inspection of multilayer defects on EUV masks," *Proc. SPIE* **5751**, 651–659 (2005).
2. Y. Liu, A. Barty, E. Gullikson, J. S. Taylor, J. A. Liddle, O. Wood, "A dual-mode actinic EUV mask inspection tool," *Proc. SPIE* **5751**, 660–669 (2005).
3. A. Barty, K. A. Goldberg, P. Kearney, S. B. Rekawa, B. LaFontaine, O. Wood II, J. S. Taylor, H.-S. Han, "Multilayer defects nucleated by substrate pits: a comparison of actinic inspection and non-actinic inspection techniques," *Proc. SPIE* **6349**, 63492M (2006)
4. K. A. Goldberg, A. Barty, H. Han, S. Wurm, *et al.* "Comparison of actinic and non-actinic inspection of programmed defect masks" presented at the *2006 International Symposium on Extreme Ultraviolet Lithography*, Barcelona, Spain, October 18, 2006.
5. K. A. Goldberg, A. Barty, Y. Liu, *et al.*, "Actinic Inspection of EUV Programmed Multilayer Defects and Cross-Comparison Measurements," *J. Vac. Sci. & Technol. B* **24** (6), 2824–2828 (2006).
6. *TEMPEST-3D* is developed by the A. Neureuther group, Department of EECS, Univ. Calif. Berkeley.
7. T. Liang, E. Frendberg, D. Bald, M. Penn, and A. Stivers, "E-Beam Mask Repair: Fundamental Capability and Applications," *Proc. SPIE* **5567**, 456–466 (2004).
8. K. Edinger, V. Boegli, W. Degel, "Performance results from the Zeiss/NaWoTec MeRit MG electron beam mask repair tool," *Proc. SPIE* **5853**, 361–370 (2005).
9. S. P. Hau-Riege, A. Barty, P. B. Mirkarimi, S. Baker, *et al.* "Repair of phase defects in extreme-ultraviolet lithography mask blanks," J. Appl. Physics **96** (11), 6812–6821 (2004).
10. A. Barty, P. B. Mirkarimi, D. G. Stearns, D. Sweeney, H. N. Chapman, M. Clift, S. Hector, M. Yi "EUVL mask blank repair", Proc *SPIE* **4688**, 385–394 (2002).
11. E. M. Gullikson, E. Tejnil, K.-Y. Tsai, A. R. Stivers, H. Kusunose, "Modeling the defect inspection sensitivity of a confocal microscope," *Proc. SPIE* **5751**, 1223–1229 (2005).
12. K.-Y. Tsai, E. Gullikson, P. Kearney, A. Stivers, "On the sensitivity improvement and cross-correlation methodology for confocal EUV mask blank defect inspection tool fleet," *Proc. SPIE* **5992**, 1178–1186 (2005).
13. Y. Tezuka, M. Itoa, T. Terasawa, T. Tomie, "Actinic Detection and Signal Characterization of Multilayer Defects on EUV Mask Blanks," *Proc. SPIE* **5567**, 791–799, 2004.
14. T. Tanaka, Y. Tezuka, and T. Terasawa, "Detection signal analysis of actinic inspection of EUV mask blanks using darkfield imaging," *Proc. SPIE* **6152**, 61523U, (2006).
15. Hamamoto, Y. Tanaka, T. Yoshizumi, Y. Fukushima, *et al.*, "Phase defect observation using an EUV microscope," *Proc. SPIE* **6151**, 615119 (2006)
16. SEMI P38-1103, "Specification for absorbing film stacks and multilayers on extreme ultraviolet lithography mask blanks," November 2003. Available at www.semi.org